Nuclear Engineering and Design 411 (2023) 112426

Contents lists available at ScienceDirect

Nuclear Engineering and Design

journal homepage: www.elsevier.com/locate/nucengdes

A modelling methodology for the description of helium behaviour accounting for the grain-size distribution

D. Pizzocri [a], A. Cechet [a], L. Cognini [a], A. Magni [a], A. Schubert [b], P. Van Uffelen [b], T. Wiss [b], L. Luzzi [a,*]

[a] Politecnico di Milano, Department of Energy, Nuclear Engineering Division, Via La Masa 34, 20156 Milano, Italy
[b] European Commission, Joint Research Centre (JRC), Karlsruhe, Germany

ARTICLE INFO

Keywords:
Helium behaviour
Grain-size distribution
Nuclear fuel
SCIANTIX

ABSTRACT

Physics-based meso-scale models of fission gas behaviour for fuel performance codes currently consider only the average grain size as physical parameter to describe the fuel microstructure. Nevertheless, information on the grain-size distribution is available for several metallographically characterized fuel samples. To extend the current modelling approach, we present new experimental data and develop a methodology to treat the fuel grain-size distribution based on multi-grain analysis. This is applied to describe helium behaviour from infused and annealed polycrystalline UO_2 samples. The methodology consists of three steps: (1) Acquisition of the empirical grain distribution from sections of the polycrystals, (2) Calculation of the gas distribution factor pertaining to each grain size class after helium infusion, and (3) Simulation of the experimental annealing histories with input parameters weighted by the gas distribution factors. To perform the multi-grain analysis, we used the SCIANTIX code, which allows calculating the helium kinetics in a single fuel grain. The application of this methodology is promising because it can represent the dynamics of helium release more consistently with the physics of the fuel microstructure compared to the state-of-art approaches, and it can be suitable for application in fuel performance codes for different enhanced accident tolerant fuel concepts as outlined in our conclusions.

1. Introduction

Helium production and behaviour in the fuel concur with volatile fission products (xenon and krypton) to gaseous swelling and release of gas, potentially affecting the integrity of the fuel rod and leading to release of volatile radioactive isotopes in the environment (El-Atwani et al., 2017; Olander, 1976; Sauvage et al., 2005). During irradiation of MOX (Botazzoli et al., 2011) and Minor Actinide MOX (MA-MOX) fuels, the initial enrichment in plutonium and actinides leads to higher helium production in reactor with respect to conventional UO_2 in pressurized water reactor (Cechet et al., 2021). Moreover, in storage conditions helium is continuously produced via α-decay of actinides and can lead to modifications of the conditioned nuclear waste microstructure, even if conservative considerations by Ferry and coauthors showed that the integrity of the fuel matrix is ensured up to the eventual breach of the canister (Ferry et al., 2010). The assessment in fuel performance codes of the effects of helium during irradiation of MOX and MA-MOX and during long-term storage of nuclear fuel is thus mandatory for the inherent safety of the future nuclear technologies (GIF, 2020). In addition, during reactor operation and transient conditions, nuclear fuel is subject to high temperature and steep temperature transients that lead to the growth of the fuel average grain size (Ainscough et al., 1973; Van Uffelen et al., 2013; Veshchunov, 2000). This affects the intra-granular fission gas behaviour in three ways, i.e., (1) increasing the average diffusion distance for gas atoms generated in the grains, thus hindering gas transport to the grain boundaries, (2) through grain boundary sweeping, which provides an additional mechanism for the collection of gas atoms at the grain boundaries (Pastore et al., 2015; El-Saied and Olander, 1993), and (3) by affecting the surface-to-volume ratio of fuel grains and consequently their gas storing capacity (Verdolin et al., 2021; Pastore et al., 2015; Pastore et al., 2013).

To model grain growth coupled with fission gas behaviour, fuel performance codes rely either on empirical models based on correlations or on physics-based models. In this second option, the models can be embedded in the code or provided by fission gas behaviour modules coupled with them, e.g., SCIANTIX (Pizzocri et al., 2020), MFPR (Veshchunov et al., 2007), MARGARET (Noirot, 2006) and CARACAS

* Corresponding author.
E-mail address: lelio.luzzi@polimi.it (L. Luzzi).

https://doi.org/10.1016/j.nucengdes.2023.112426
Received 13 February 2023; Received in revised form 8 May 2023; Accepted 6 June 2023
Available online 22 June 2023

Nomenclature

a^i(nm)	Average grain radius in each grain size class
$a_{exp}{}^i$(m)	Experimental average grain radius in each grain size class
β(s^{-1})	Trapping rate
c_{exp}(at m^{-3})	Experimental helium concentration released after the annealing
c^i(at m^{-3})	Helium concentration in solution in each grain size class
c_0^i(at m^{-3})	Initial helium concentration in solution in each grain size class
C_{sat}(at m^{-3})	Guess of helium solubility for the infusion model
$\overline{D}$(nm)	Average grain diameter
D_0^i(nm)	Initial average grain diameter in each grain size class
D^i(nm)	Average grain diameter in each grain size class
$\overline{D}_0$(nm)	Initial average grain diameter
D_{He}(m^2 s^{-1})	Helium diffusivity
E_A(J)	Activation energy of helium diffusivity
F_{He}(/)	Fractional helium release
$F_{He}{}^i$(/)	Fractional helium release pertaining to each grain size class
$f_g{}^i$(/)	Helium distribution factor in each grain size class
γ(s^{-1})	Thermal re-solution rate
h	Spatial mode index (see N)
k(nm^4 h^{-1})	Grain boundary mobility
k_0(nm^4 h^{-1})	Pre-exponential factor of the grain boundary mobility in Arrhenius law
k_B(J K^{-1})	Boltzmann constant
k_H(at m^{-3} MPa^{-1})	Helium-UO_2 Henry's constant
m^i(at m^{-3})	Helium concentration in bubbles in each grain size class
N_g	Total number of grains measured per sample
N^i	Number of grains in each grain size class (i.e., the grain size distribution)
N_{exp}^i	Experimental grain size distribution
N	Number of spatial modes in solution of the diffusion equation
n_g	Number of classes in the grain size distribution
p_{inf}(MPa)	Experimental infusion pressure
Q(eV)	Activation energy of the grain boundary mobility in Arrhenius law
r(m)	Radial coordinate along the grain (assumed as spherical)
σ	Standard deviation of the grain boundary mobility fitting parameters (see k_0 and Q)
R_{He}(at m^{-3} s^{-1})	Helium release rate
$R_{He}{}^i$(at m^{-3} s^{-1})	Helium release rate pertaining to each grain size class
t(s)	Time
T(K)	Temperature
T_{room}(K)	Room temperature
T_{inf}(K)	Experimental infusion temperature
t_{inf}(s)	Experimental infusion time

(Jomard et al., 2014), that directly solve the differential equations that describe the gas-related phenomena. In addition, the models included in these modules are based on parameters related to the microstructure of the fuel which are trained with data obtained from lower-scale simulations (Parks et al., 2017; Govers et al., 2009; Van Brutel and Chartier, 2019). This physics-based approach, compared to classical correlation-based approaches, generally requires more computational time, more rigid convergence criteria of the employed numerical methods, and introduces many physical parameters, whose uncertainty weighs heavily on the results. However, the correlation-based approach is limited to the temperature and burnup ranges in which the data were collected, while the physics-based models can be easily extended to new scenarios like other types of fuel and temperature transients (Pastore et al., 2013; Williamson et al., 2016; Van Uffelen et al., 2011). For their flexibility, mechanistic models are nowadays being implemented in fuel performance codes (Pastore et al., 2013; Van Uffelen et al., 2011; Tonks et al., 2017).

A current limitation of such physics-based approach in meso-scale fission gas behaviour modules for fuel performance codes is that it considers only the average fuel grain size as physical parameter to describe fuel microstructure, without considering the grain size distribution (Ainscough et al., 1973; Van Uffelen et al., 2013; Veshchunov, 2000; Mendelson, 1969; Yao et al., 2017; Bouëxière et al., 2019). The small fuel grains have higher diffusion rates with respect to the bigger ones and this can bring to unbalanced gas kinetics during irradiation or annealing, that leads to a different gas release dynamics in time (Lösönen, 2000). Thus, modelling this physical effect can refine the state-of-art of physics-based modelling of inert gas in fuel performance codes. In addition, this refinement allows building a relation between fuel physical properties at the nano-scale and macroscopic properties, whose understanding is fundamental for the safety and efficiency of nuclear fuel (Parrish and Aitkaliyeva, 2018).

The work by Millett and coauthors (Millett et al., 2013) analysed the effect of considering a grain-size distribution instead of an average grain-size for the calculation of diffusion-based fission gas release. They generated virtual samples with Hillert grain-size distribution and solved the diffusion problem in each grain assuming both annealing conditions, i.e., no gas production, and irradiation conditions, i.e., uniform and constant gas production. They pointed out that using an average grain size implies a systematic deviation from the release observed in a polycrystalline sample.

In this work, we propose a methodology to model the effects of grain distribution on helium behaviour in polycrystalline UO_2 samples. The proposed methodology is intended to extend the previous work by Millett and coauthors by including a non-zero Dirichlet boundary condition, which is critical in view of the high solubility of helium in oxide fuels, and to be applicable with any grain-size distribution, such as the lognormal grain-size distribution observed in the high burnup structure (Cappia et al., 2016; Spino et al., 1996).

Even if the applicability under irradiation of the new model for helium behaviour must still be demonstrated, testing the subset of capabilities/parameters suitable for UO_2 fuel in annealing conditions allows for a more progressive and trustable model development process. The methodology application is showcased on fuel samples infused with helium and annealed with a temperature ramp up to 1800 K (Cognini, 2021), for which characterization of the grain-size distribution is available in all steps. The results have been obtained with SCIANTIX (Pizzocri et al., 2020), a meso-scale module for fission gas and helium behaviour designed to be either stand-alone (Cechet et al., 2021; Cognini et al., 2021) or to be coupled with fuel performance codes (Pizzocri et al., 2019). SCIANTIX solves the kinetics of inert gases at the scale of a single fuel grain, thus running multiple SCIANTIX simulations is suitable to perform such multi-grain analysis.

The methodology consists of three steps: (1) acquisition of the empirical grain distribution from SEM images of the polycrystals, (2) calculation of the gas distribution factor pertaining to each grain size class after helium infusion, and (3) simulation of the experimental annealing histories with input parameters weighted by the gas distribution factors. This methodology is applicable to fuel performance codes since it consists of running a set of simulations with different correlated input parameters and a final summation on the variables of interest. Moreover, it is easily extendable to other scenarios, like helium

Table 1
Average grain diameter of the samples from Cognini (Cognini, 2021) at the different steps described in Section 2 and experimental data and conditions of the sample from Miao et al. (Miao et al., 2017) used in this work. The considerable difference in the measurements uncertainties among the results of Cognini (Cognini, 2021) and the ones by Miao et al. (Miao et al., 2017) arises from the different experimental technique used, linear intercept on SEM images and synchrotron wide-angle X-ray scattering.

Sample	Initial grain diameter (nm)	Infusion time (h)	Infusion temperature (K)	Grain diameter after infusion (nm)	Grain diameter after annealing (nm)
A22 (Cognini, 2021)	331 ± 52	6	1123	335 ± 52	2538 ± 412
A32 (Cognini, 2021)	216 ± 42	6	1123	254 ± 56	–
B12 (Cognini, 2021)	292 ± 52	2	1123	332 ± 42	–
C21 (Cognini, 2021)	521 ± 72	2	1253	560 ± 78	2330 ± 378
Miao et al., #1 (Miao et al., 2017)	144 ± 1	7.5	1003	–	147 ± 2
Miao et al., #2 (Miao et al., 2017)	144 ± 1	7.5	1093	–	181 ± 6

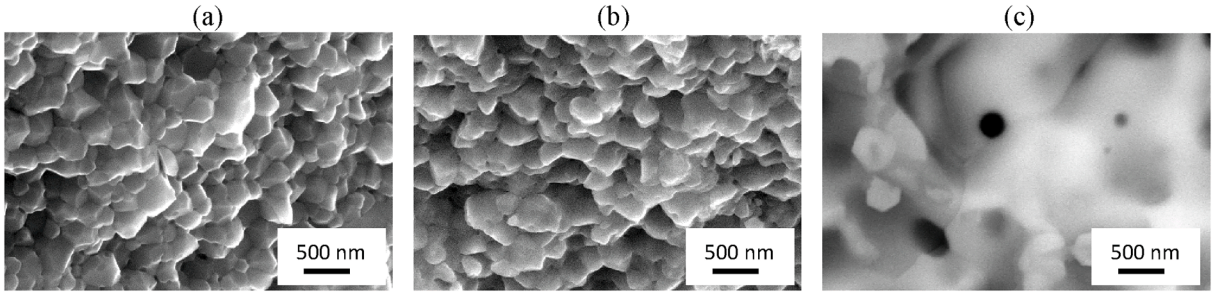

Fig. 1. SEM images of sample A22 microstructure at the different steps along the experiment: (a) after preparation/before infusion, (b) after infusion/before annealing, (c) after annealing (Cognini, 2021).

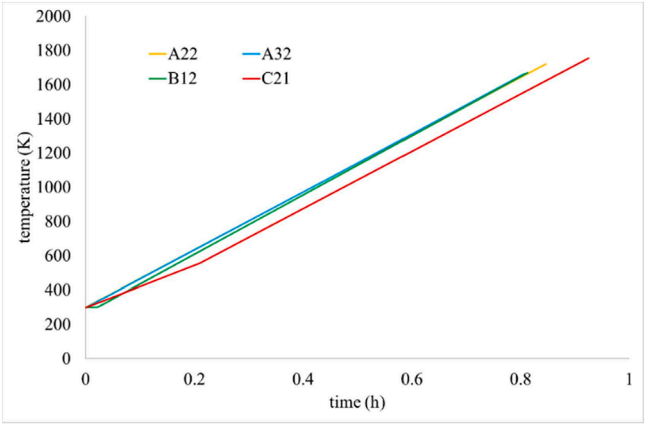

Fig. 2. Annealing temperature ramps of the nanograined samples (Cognini, 2021).

implanted and samples doped with an α-emitter (Talip et al., 2014; Talip et al., 2014), together with other fuels and different microstructures.

Accompanying the proposed methodology, we present a new model to predict the grain growth of stoichiometric nanograined polycrystalline UO_2 samples in the range 1003 − 1253 K. The development of this model was necessary to extend state-of-the-art grain growth models with respect to this type of microstructure (Yao et al., 2017; Miao et al., 2017; Tonks et al., 2021).

The manuscript is structured as follows: in Section 2, we describe the UO_2 polycrystalline samples and the different stages of their experimental analysis. In Section 3 we focus on the methodology to treat the grain size distribution in the samples, while Section 4 details the grain size evolution of the considered samples, providing information for the application of the methodology itself. In Section 5, we apply the proposed methodology to helium infused and released from four samples. The conclusions, the limitations and the foreseen further developments are drawn in Section 6. Further details on the hypothesis of the proposed grain growth model in nanograined annealed polycrystals are reported in Appendix.

2. Description of the samples

Uranium dioxide polycrystals were prepared at JRC-Karlsruhe laboratories from nano-powders using two different Spark Plasma Sintering (SPS) techniques that allowed to obtain nanograined fuel microstructure, namely: High-Pressure SPS (HP-SPS) and 2 steps SPS (2S-SPS) (Cognini, 2021; De Bona et al., 2021). The samples featured a theoretical density up to 95% and grains in the nanometric range. No deviation from the stoichiometry was ensured by means of X-Ray Diffraction (XRD) analysis of sintered samples. For an extensive description of the sample preparation process, including XRD results prior and after sintering and after reduction in Ar-H_2 atmosphere, we refer the reader to (Cognini, 2021). The polycrystals were then classified into four classes depending on their grain size, namely: A (≈250 nm), B (≈ 400 nm), C, (≈600 nm) and D (≈1500 nm).

After the preparation and characterization, the samples were infused with helium by means of an autoclave at an infusion temperature kept constant in time and uniform over the sample by means of a laser beam. The infusion lasted 2 or 6 h, depending on the sample. The samples were then kept at ambient temperature for several hours and then moved to a Thermal Desorption Mass Spectrometer (TDMS), in which they were annealed in vacuum conditions up to 1873 K with a temperature ramp of 30 K min^{-1}. During the annealing, the helium released from the sample was monitored, then discharged from the TDMS and collected by pumping in a high-pressure chamber. Finally, it was measured by means of Quantitative GAs MEasurement System (Q-GAMES) and its signal compared with a reference spike of a defined quantity of helium. At the end of the heating phase, the samples were cooled down to room temperature. In the following analysis, the focus is going to be on sample B12 (Table 1), for which complete online information in terms of helium release and helium release rate is available along the annealing phase.

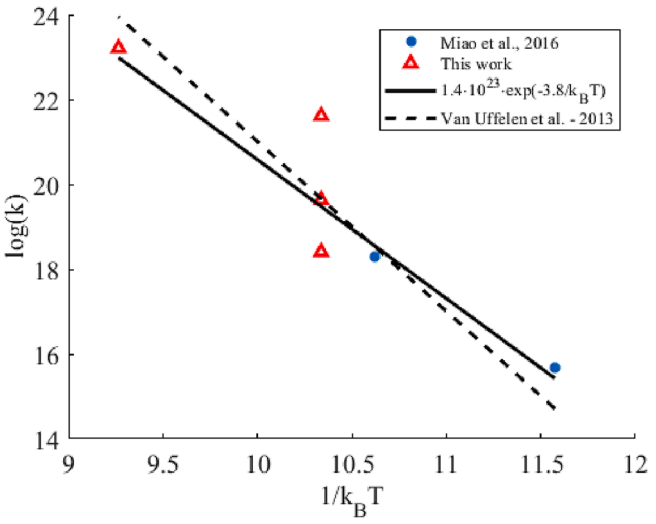

Fig. 3. Experimental data and fitting of the grain boundary mobility. For the sake of comparison, the correlation for the grain boundary mobility from Van Uffelen et al. (Van Uffelen et al., 2013) is also included, representing a reference correlation applied in fuel performance codes.

SEM images were acquired (area of 100 μm^2, HFW = 11.8 μm, WD = 10.0 mm (Cognini, 2021)) after sample preparation/just before the infusion, after the infusion/before the annealing for samples A22, A32, B12 and C21. In addition, SEM images were acquired also after the thermal desorption, for samples A22 and C21. We obtained the mean grain diameter of the aforementioned polycrystalline samples at the different stages, when SEM images were available, by measuring 240 linear intercepts per sample section using the ImageJ software, then converting them to equivalent spherical diameters (Mendelson, 1969). The uncertainties on the experimental grain diameters have been obtained considering both the uncertainty on the data and of ImageJ software and a recovery factor of 2.5 to consider the non-polished surface and camera misalignment (ASTM, 2018). The average grain diameters obtained are reported in Table 1, together with the measurement results reported by Miao and coworkers on similar nanocrystalline fuel samples (Miao et al., 2017), which are included in the following analysis. SEM images corresponding to each stage of sample A22 are shown in Fig. 1, to illustrate the typical microstructure of the samples considered. The annealing temperature ramps for such samples are reported in Fig. 2. It is worth noting that the average grain size in the samples we considered is in the order of hundreds of nanometres compared to tens of microns of the typical grain size in an oxide fuel pellet. This size discrepancy translates in shorter diffusion length to be travelled by atoms within the sample, and has implications in the time-dependent gas behaviour within the sample.

The dataset reported in Table 1 has been used to obtain the grain growth model used in this work. Since the infusion is realized at constant temperature, we used the measured grain diameters before and after the infusion to evaluate the grain growth as a function of the infusion temperature. Following Botazzoli (Botazzoli, 2011) the evolution of the mean grain diameter for the samples under analysis, $\overline{D}$ (nm), is best described by:

$$\frac{d\overline{D}}{dt} = \frac{k}{4\overline{D}^3} \tag{1}$$

where the grain boundary mobility $k = k_0 \exp(-Q/k_B T)$ is derived by fitting. The proposed correlation for the grain boundary mobility is reported in Fig. 3 and the values of the fitting parameters and the corresponding confidence interval at 95% (in brackets) are k_0(nm^4 h^{-1}) = 1.4 10^{23} (2.3 10^{19}; 8.7 10^{26}) and Q (eV) = 3.8 (1.2; 5.3). The value of the R^2 for the fitting of the grain boundary mobility is 0.83. Considering the confidence intervals on the fitting parameters, the proposed correlation is compatible with the one by Van Uffelen (Van Uffelen et al., 2013) for unirradiated MOX fuel samples (see Fig. 3), which is a reference correlation applied in fuel performance codes.

3. Methodology

In this work, we propose a new methodology to consider the effect of the grain size distribution to extend the physics-based approach in the modelling of inert gas behaviour in oxide fuel. We apply it to describe intra-granular helium kinetics in the polycrystalline UO_2 samples mentioned in Section 2, since for these samples extensive information about their grain-size distribution was available, but it can easily be extended to the physical description of other gases and sample microstructures.

The methodology consists of three steps. First, we measured N_g linear intercepts from SEM images of as-fabricated samples and we converted them to grain diameters considering the sphere as equivalent shape of the grain. Then these grain diameters were divided into n_g classes[1], defining the number of grains per class N^i (i.e., the grain diameter distribution), from which the average grain diameter D^i and the corresponding average grain radius a^i are defined in each grain size class.

The second step is the modelling of infusion of helium inside the fuel grains. This problem is mathematically described by a diffusion equation in a spherical geometry with constant boundary conditions (Sung, 1967; Sung and Turnbaugh, 1968; Crank and Gupta, 1975; Rufeh et al., 1965). Given that the diffusion along grain boundaries is faster than the diffusion inside fuel grains (ratio between grain-boundary and matrix diffusivities is in the order of three order of magnitude (Giorgi et al., 2022)), it is reasonable to assume that the grain boundaries are saturated before the infusion of the grain begins. Further model-based verification of this working hypothesis is of interest and can be pursued via, e.g., using a phase-field model of the whole sample. According to the proposed methodology, we perform n_g SCIANTIX simulations, each representing the infusion of helium inside each grain size class. The boundary condition (i.e., the helium solubility) is *a priori* unknown, therefore it is necessary to estimate its value from the analytical solution of the equation, substituting the diffusion coefficient, time, grain radius distribution and temperature with the experimental value for each sample after infusion (Crank and Gupta, 1975). Before solving each of the n_g equations, it is necessary to divide the boundary condition by N_g. The problem is thus formally a set of diffusion equations solved for each of the n_g grain size classes:

$$\frac{\partial c^i(r,t)}{\partial t} = D_{He}\frac{1}{r^2}\frac{\partial}{\partial r}\left(r^2\frac{\partial c^i(r,t)}{\partial r}\right) with\ i \in [1, n_g] \tag{2}$$

with the boundary conditions:

$$\begin{cases} c^i(a^i,t) = \dfrac{C_{sat}}{N_g} \\ c^i(r,0) = 0 \\ \left.\dfrac{\partial c^i}{\partial r}\right|_{r=0} = 0 \end{cases} \tag{3}$$

in which the solubility C_{sat} (at m^{-3}) is estimated as:

$$C_{sat} = \frac{c_{ann}}{1 - \frac{6}{\pi^2}\sum_{i=1}^{n_g}\sum_{h=1}^{N}\frac{1}{h^2}\frac{N^i_{inf}}{N_g}\exp\left(-\frac{h^2\pi^2 D_{He}(T_{inf})t_{inf}}{{a_{inf}}^{i2}}\right)} \tag{4}$$

where c_{ann} (at m^{-3}) is the helium concentration measured as released

[1] The empirical rule $n_g = \sqrt{N_g}$ has been applied to obtain a significant number of classes.

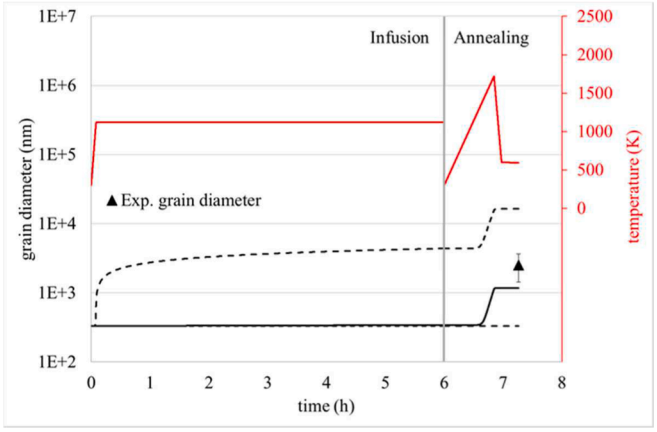

A22 (a)

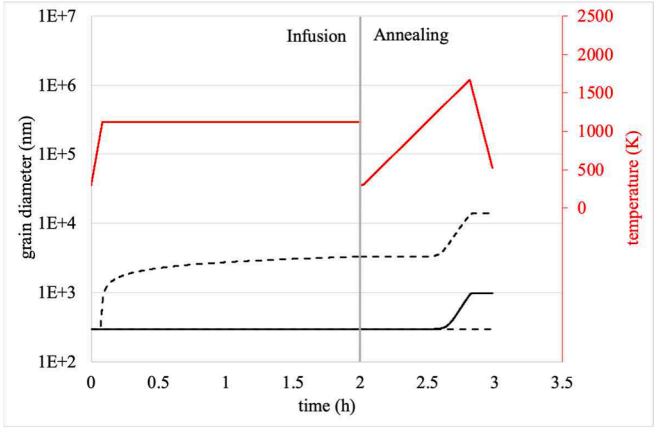

B12 (b)

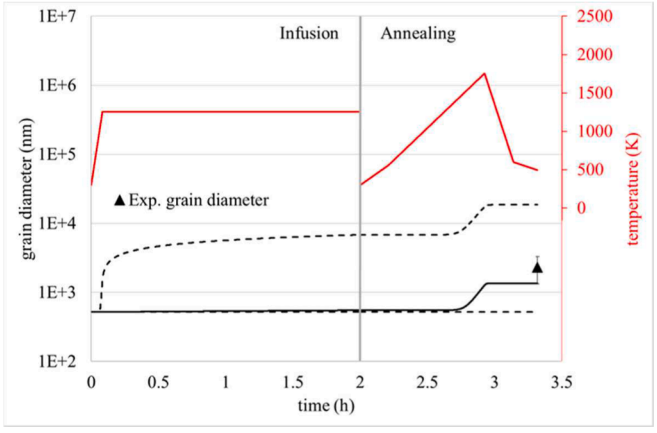

C21 (c)

Fig. 4. Application of the grain growth model presented in this work in the A22 (a), B12 (b), and C21 (c) samples (infusion/annealing temperature depicted in the red curves). The solid black curves represent the evolution of the grain diameter obtained with the best fit model parameters and the dashed lines represent respectively the upper and lower boundary of the average grain diameter, considering the confidence interval on the pre-exponential factor and on the activation energy of the grain boundary mobility.

after annealing, under the assumption that the annealing phase releases all the gas infused in the samples, i.e., $c_{ann} = c_{inf}$, T_{inf} (K) is the experimental infusion temperature, t_{inf} (s) is the experimental infusion time, N^i_{inf} is the experimentally measured grain size distribution after infusion,

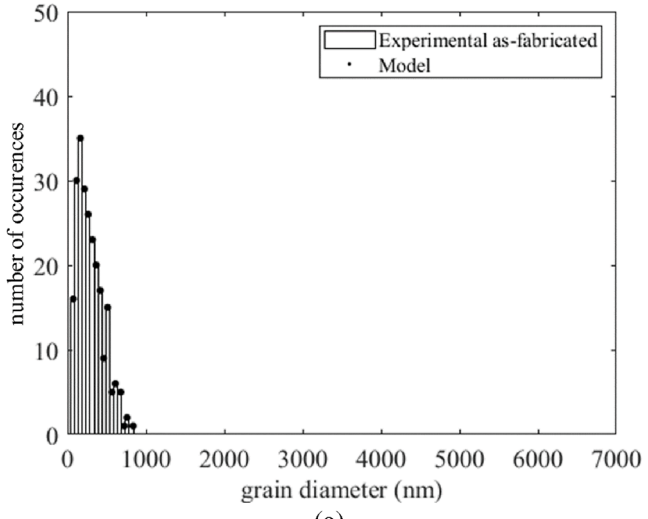

(a)

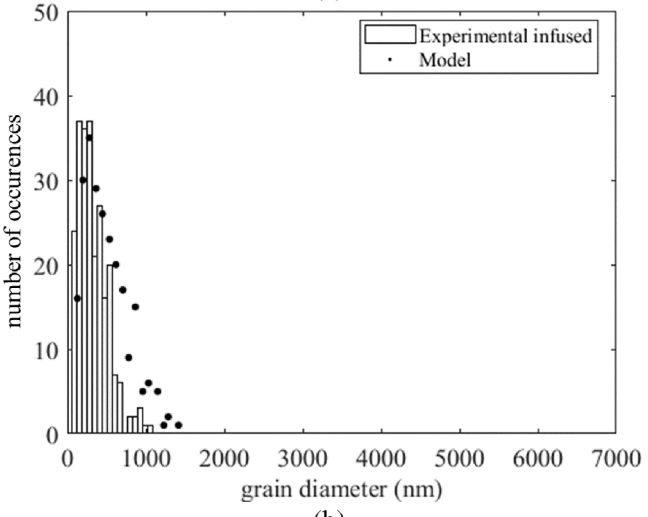

(b)

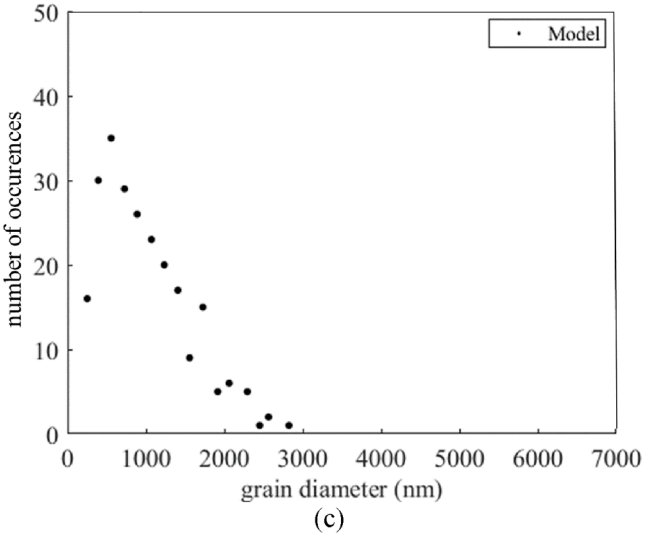

(c)

Fig. 5. Grain size distribution of the B12 sample at the end of the three stages: fabrication (a), infusion (b), and annealing (c). The histograms correspond to the measured grain-size distribution and the black dots correspond to the grain growth model results following Eq. (1) (under the hypothesis described in the Appendix).

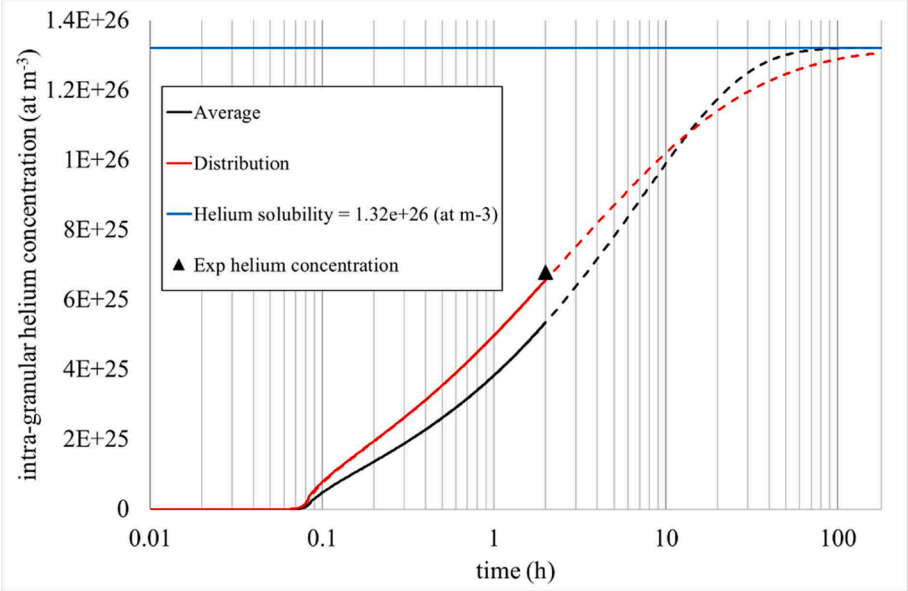

Fig. 6. Evolution of intra-granular helium concentration in sample B12. The black curve represents the evolution using solely the average grain size, whereas the red curve represents the result obtained considering the grain-size distribution via the herein proposed methodology. The solid lines describe experimental infusion time (2 h), whereas the dashed line prolong the simulation up to 180 h of infusion, when saturation is reached (blue line).

$a_{inf}{}^i$ (m) is the corresponding grain radius of each grain size class and the summation is carried on considering $N = 40$ modes. The diffusion coefficient D_{He} ($m^2\ s^{-1}$) used for this analysis is the one recommended by Luzzi et al. (Luzzi et al., 2018) for infused samples.

The total helium concentration inside the grains is obtained by summing up all the n_g concentrations calculated with Eq. (2), each weighted by N^i. The outcomes of this step are the gas distribution factors $f_g{}^i$, i.e., the fractions of the total gas retained by each grain size class after infusion, defined by the ratio:

$$f_g{}^i = \frac{N^i c^i(t = t_{inf})}{\sum_{i=1}^{n_g} N^i c^i(t = t_{inf})} \tag{5}$$

The third step is the simulation of intra-granular helium behaviour during the annealing of the polycrystalline samples. We performed n_g simulations in SCIANTIX with the initial intra-granular helium concentration weighted by the gas distribution factor pertaining to each grain size class. Finally, we obtain the quantity of interest by summing up the n_g output variables. In this work, we considered the fractional helium release and helium release rate as figures of merit to compare the experimental database with the SCIANTIX results, which have the following final expressions:

$$F_{He} = \sum_{i=1}^{n_g} F_{He}{}^i \tag{6}$$

$$R_{He} = \sum_{i=1}^{n_g} R_{He}{}^i$$

where F_{He} (/) is defined as the ratio between helium released (at m^{-3}) and initial helium in grains (at m^{-3}), R_{He} (at $m^{-3}\ s^{-1}$) is the rate of helium release, and $F_{He}{}^i$ and $R_{He}{}^i$ are the same quantities pertaining to each grain size class.

4. Grain-size evolution

Fig. 4 presents the application of the grain growth model proposed in Section 2 (Fig. 3) on A22, B12, and C21 infusion and annealing histories. Since the proposed grain growth model is tailored on this dataset, the agreement with the final values of the experimental grain diameters is to be expected. The slight underprediction of the final value of the grain diameter is ascribed to the fact that the temperature range of the model is limited to 1253 K (Table 1) while the annealing temperature reaches ≈1800 K. Further experiments with nanograined UO_2 stoichiometric samples annealed, extending the present temperature range, can be useful to throw light on the grain growth process of such nanostructure.

Due to the spread in the data, which is reflected in wide confidence intervals of the parameters of the grain boundary mobility, we performed the simulations using the upper and lower boundary of the pre-exponential factor and the activation energy to evaluate the degree of overlap of the modelled grain growth and the experimental data (Fig. 4).

Lastly, we report the evolution of the grain-size distribution as predicted by the proportional application of the grain growth model to each grain-size class (Fig. 5). This working hypothesis is further detailed in the Appendix, together with the results of the evolution of the grain-size distributions of the other samples. For the sake of brevity, the result is herein reported only for the B12 sample, on which the proposed methodology is applied in the next Section. This knowledge of the evolution of the grain-size distribution is the fundamental starting point for the application of the proposed methodology.

5. Application of the proposed methodology

Without loss of generality, we apply the methodology proposed in the previous Section to the B12 sample, for which data on the grain-size distribution (Figs. 4, 5) are available together with data concerning the helium release and the helium release rate during annealing.

The simulated results in terms of helium release rate and fractional release have been obtained with the intra-granular helium behaviour model embedded in SCIANTIX (Cognini et al., 2021). The model describes the intra-granular helium behaviour by including its production from actinide α-decays, ternary fissions and (n,α)-reactions with ^{16}O (Cechet et al., 2021), intra-granular diffusion, trapping of helium into intra-granular bubbles, irradiation re-solution, helium solubility (Veshchunov, 2000; Lösönen, 2000; Cognini et al., 2018) and thermal re-solution of gas from the bubbles back into the fuel matrix. In this work, the model is tailored to describe helium behaviour in infused samples subjected to a short annealing transient; thus, helium production is negligible and irradiation re-solution of bubbles has been

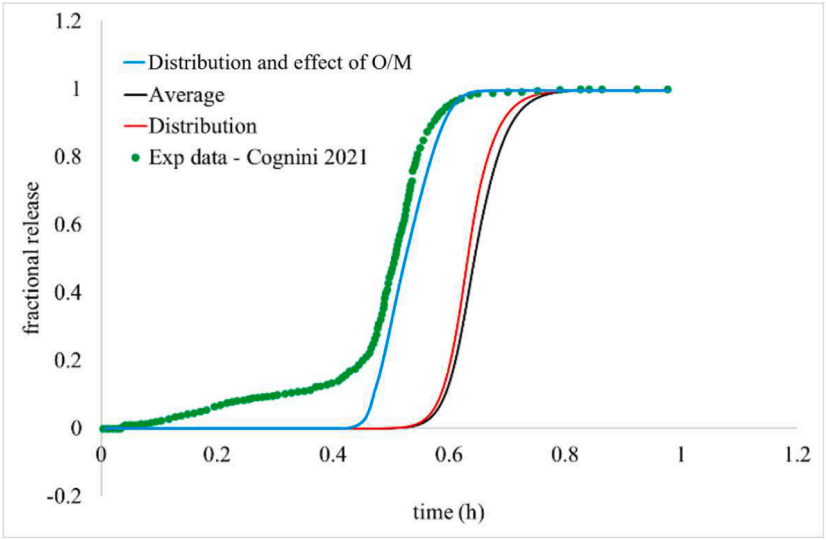

(a)

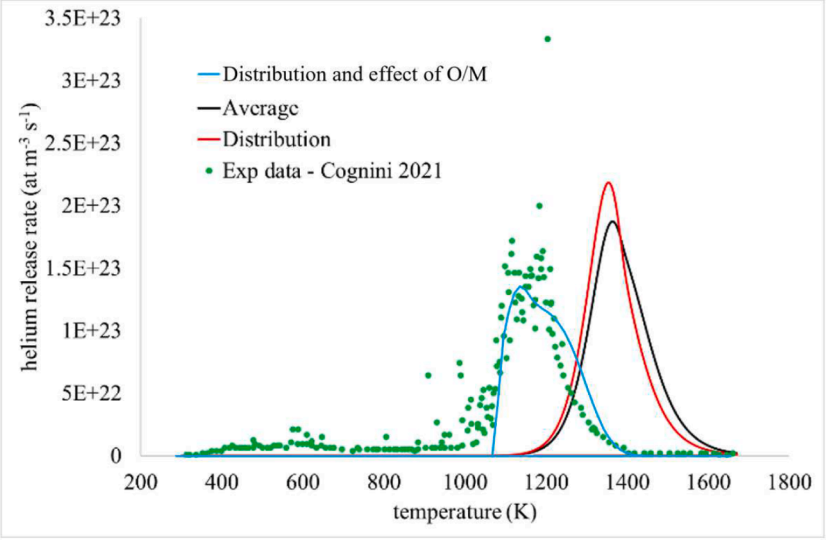

(b)

Fig. 7. Comparison of fractional helium release (a) and helium release rate (b) with experimental data from sample B12. The red curve is the SCIANTIX result obtained with the proposed methodology, including the grain-size distribution effect, and the black curve is the SCIANTIX result obtained with solely the average grain size. The light-blue curve shows the effect of the deviation from stoichiometry.

neglected. The coupled equations of the model applied in this analysis are the following:

$$\begin{cases} \dfrac{\partial c^i}{\partial t} = D_{He}\nabla^2 c^i - \beta c^i + \gamma m^i \\ \dfrac{\partial m^i}{\partial t} = \beta c^i - \gamma m^i \end{cases} \tag{7}$$

where the quantities are related to each grain size class: c^i (at m^{-3}) is the concentration of helium in solution, m^i (at m^{-3}) is the concentration of helium in bubbles, β (s^{-1}) is the trapping rate proposed by Ham (Ham, 1958), and γ (s^{-1}) is the thermal re-solution rate as proposed by Cognini et al (Cognini et al., 2021).

The main modelling assumptions necessary to set up each SCIANTIX annealing simulations are the following:

1. The initial concentration of helium in solution at the beginning of the annealing steps, which is a fraction of the overall infused helium concentration, has been calculated from Henry's law $c_0^i = k_H p_{inf}$ at room temperature T_{room}, where p_{inf} (MPa) is the infusion pressure and k_H (at m^{-3} MPa^{-1}) is Henry's constant for single crystals (Cognini et al., 2018). The excess helium concentration is assumed to be precipitated in intra-granular bubbles during the period at room temperature.
2. Helium bubble density is in the range 10^{20}–10^{22} (bub m^{-3}) as reported by various studies (Talip et al., 2014; Schwartz et al., 2005). We therefore impose the value of 10^{21} (bub m^{-3}). This assumption could be confirmed via further experimental investigation of the samples after the infusion process.
3. Single-sized intra-granular bubbles are considered, by dividing the initial helium concentration (Barani et al., 2019).

Moreover, paired with the grain growth model presented in Section 2, grain boundary sweeping has been applied in this analysis (European Commission, 2022; Pastore et al., 2015). It is also assumed that helium is

instantaneously released when reaching grain boundaries, in line with (Cognini et al., 2021). This hypothesis is only justifiable during the annealing transient in vacuum conditions, and formally corresponds to enforcing a null boundary condition (no helium pressure) at the grain boundaries, ensuring no re-absorption of the helium released from the grain interior. In non-vacuum conditions (e.g., during the infusion step of the experiment, or for the modelling of in-pile helium behaviour) one needs to consider the concentration of helium at grain boundaries (Botazzoli, 2011).

This set of hypotheses calls for several limitations still hindering the current intra-granular helium behaviour modelling. These limitations are planned to be addressed in future works:

- No explicit treatment of helium bubble nucleation is present, i.e., only *one-off bubble nucleation* is considered. To include an additional equation for the bubble density evolution, which is fundamental to predict the bubble formation between infusion and annealing stages, requires information about the helium solubility at room temperature and on the nucleation process[2].
- The main parameters for the intra-granular helium kinetics, i.e., helium diffusivity (D_{He}) and helium Henry's constant (k_H), are affected by high uncertainties, a factor of ten (x 10) (Luzzi et al., 2018) and a factor of a thousand (x 1000) (Cognini et al., 2018), respectively. This hinders the general applicability of the model.

In the following, we present the results of the application of the proposed methodology using SCIANTIX code on sample B12. For the sake of comparison, together with the results that include the effect of the grain-size distribution, we performed an additional SCIANTIX simulation considering the average grain size.

Fig. 6 represents the evolution of intra-granular helium concentration during the infusion phase. The solid red line represents the result obtained considering the grain size distribution during the experimental infusion time (i.e., 2 h). The small grains are filled with helium earlier than the bigger ones, so the intra-granular concentration is higher with respect to the black curve that shows the evolution of the same quantity considering the average grain radius. For the sake of completeness, we calculated the evolution of the intra-granular helium concentration up to 180 h of infusion (dashed lines). Considering the grain-size distribution indicates that the infusion kinetics is governed by the bigger grains in which saturation is not reached up to the end of the infusion (represented by the black triangle in Fig. 6) and explains why the two curves cross each other after around 10 h of infusion. This represents a first attempt to model helium infusion, whose rate strongly depends on helium diffusivity, a parameter on which a high uncertainty exists.

From the application of this methodology accounting for the effect of the grain-size distribution, it is possible to assess the infusion time suitable to reach helium saturation in the polycrystalline sample. For example, in sample B12 (Fig. 6) infused at 1123 K, the extrapolated infusion time to reach 95% of the helium saturation is around 55 h, while to reach 99% of the saturation 180 h are required. The corresponding extrapolated infusion time based solely on the average grain size is lower: 32 and 56 h for 95% and 99% of the saturation, respectively. Not considering the grain-size distribution goes in the direction of underestimating the required infusion time, resulting in the risk of a non-conservative experimental design scenario in which saturation is erroneously expected but *de facto* not reached.

Fig. 7 presents the results on helium released during annealing. For what concerns fractional helium release (Fig. 7a), the inclusion of the grain-size distribution via the proposed methodology slightly anticipates the onset of helium release with respect to the simulation with average grain size. This is due to the small grains from which helium is released earlier due to the higher diffusion rate D_{He}/a^2 with respect to the average grain size. Nevertheless, from the integral point of view of total release, the effect is minimal.

As for the release rate profiles (Fig. 7b), by applying the proposed methodology it is expected to have the peak of helium release rate at lower temperatures, i.e., closer to the experimental data compared to the simulation adopting average grain size. Complementary, the high temperature tail of the release rate peak predicted accounting for the grain-size distribution is lower than the one based solely on the average grain size, since the bigger grains exhibit a lower diffusion rate.

The overprediction of the temperature at which the peak of release rate occurs could be ascribed to a slight change in stoichiometry of the samples as they are annealed at high temperatures. The results of Yakub et al. (Yakub et al., 2010) indicate that the activation energy of helium diffusion in UO_2 decreases as the matrix composition departs from stoichiometry. By analysing the non-dimensional ratio E_A/k_BT, (with E_A (J) being the activation energy of helium diffusion, k_B (J/K) Boltzmann's constant, and T (K) the temperature) we can see that for the model to match the experimental release temperature of ≈ 1200 K, instead of the predicted ≈ 1400 K, the activation energy of helium diffusion should drop by [(1200 K – 1400 K)/1200 K] = –14%, which according to Yakub et al. (Yakub et al., 2010) is compatible with a deviation of stoichiometry of 0.01–0.02, i.e, $UO_{1.98\text{-}1.99}$. This consideration calls for the importance of controlling/assessing the samples stoichiometry in these types of experimental works. As a quantitative indication of the impact of this parameter, Fig. 7 reports the results obtained accounting for the effect of the deviation from stoichiometry on the activation energy of helium diffusivity.

These results showcase that modelling the effect of the grain-size distribution helps predicting helium behaviour with physical coherence with respect to simply considering an average grain size, without considerable impact on the computational time. Besides the effect herein described, the general overprediction of the temperature at which helium release occurred could be ascribed to the helium retained at grain boundaries, which is released with lower activation energies, or to the release of helium stored close to the sample surfaces as a result of the infusion process (Colle et al., 2014; Maugeri et al., 2009), whose

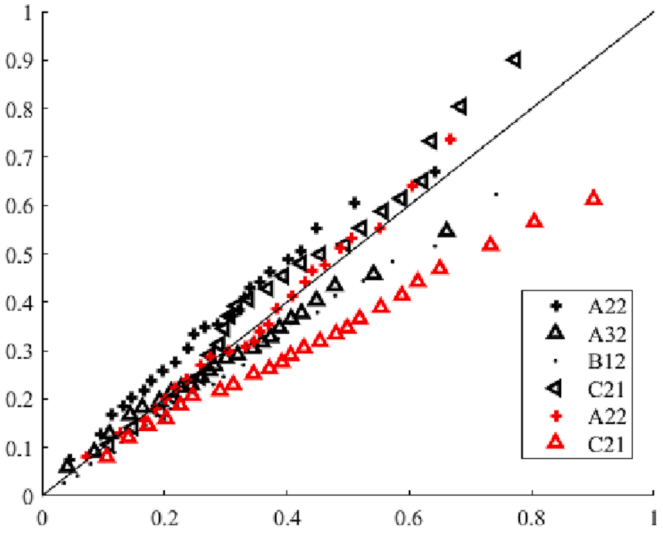

Fig. A1. Quantile-quantile plot of the normalized empirical distributions before (x-axis) and after (y-axis) infusion (black points) and annealing (red points) from the SEM images of the polycrystalline samples. Since the empirical quantiles show a limited deviation from the reference line at 45°, it indicates that the quantiles approximately come from the same distribution. Thus, considering the large uncertainties, grain growth is assumed to preserve the shape of the distribution.

[2] To acquire knowledge on the process of nucleation of helium bubbles in these conditions, it is envisaged to perform TEM investigation on the samples used in this work.

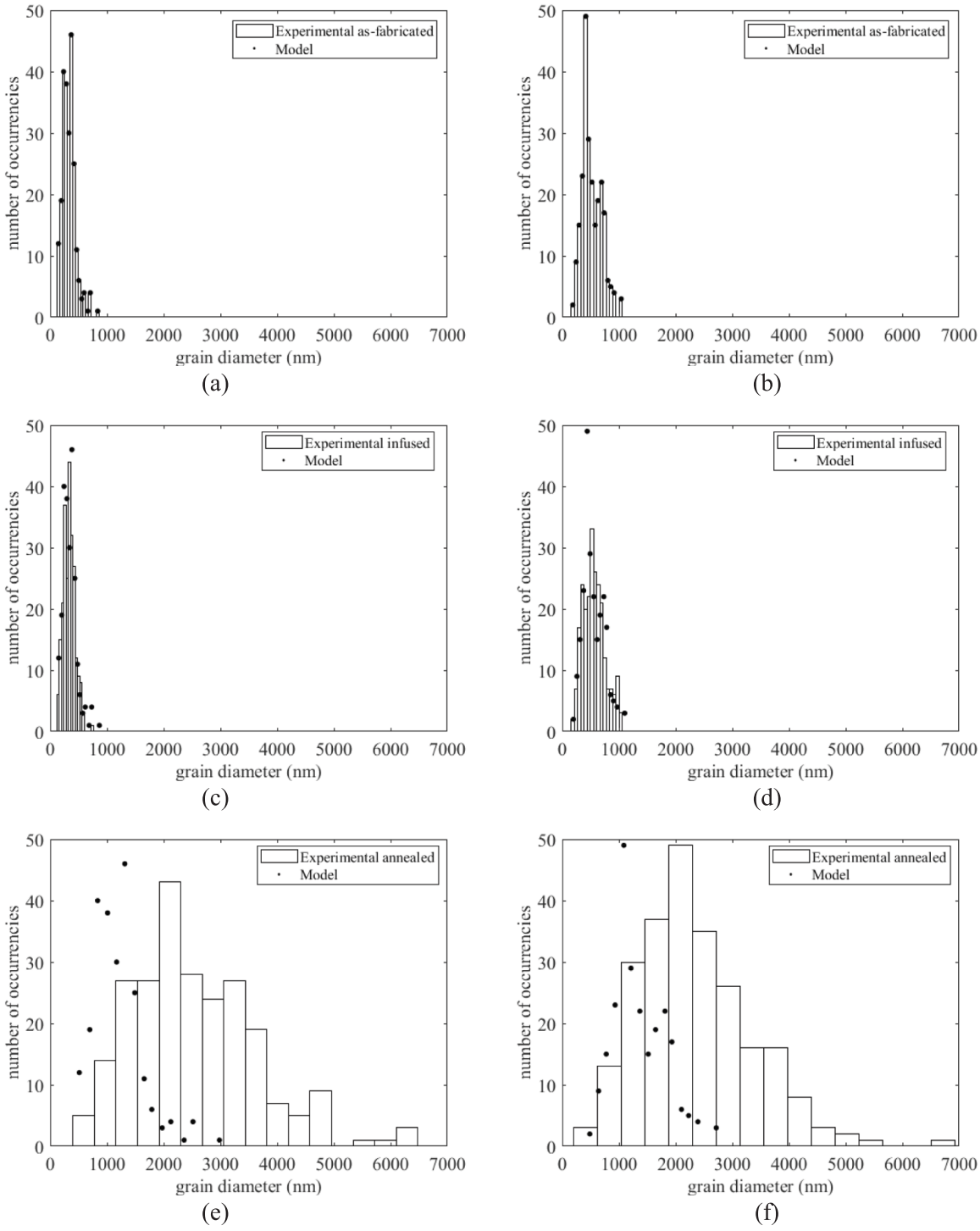

Fig. A2. Grain-size distribution of A22 (a, c, e) and C21 (b, d, f) at the end of the three stages: fabrication (a, b), infusion (c, d) and annealing (e, f). The histograms correspond to the empirical grain size distribution and the black dots correspond to the grain growth model results following Eq. (1) and Eq. (A.1).

treatment is not herein considered and is an ongoing further development of this work.

It is worth commenting that besides the limited quantitative impact on the results observed via the application of the proposed methodology to the simulation of the B12 sample infusion and annealing, more general features on the proposed approach are to be highlighted. First, by definition, accounting for the grain-size distribution effect is formally identical to removing a second-order approximation, i.e., the difference between directly using the average grain size and using the grain-size distribution and then averaging the results obtained. The impact of such approximation depends on the shape of the grain-size distribution, on its variance on its characteristics (e.g., bimodality). By observing Fig. 5, one could expect that the impact of this approximation is thus limited for sample B12, since the grain-size distribution is centred on the average value with limited variance. This implies that from the engineering point of view an *a priori* estimation of the expected impact arising from the application of this methodology can be obtained via the knowledge of the grain-size distribution itself. Secondly, the impact of

the proposed methodology is only slightly dependent on the specific grain growth model assumed (Fig. 3) if the hypotheses on the evolution of the grain-size distribution are respected (see Appendix).

Lastly, it is useful to discuss the experimental results reported in this work in relation to the annealing experiments performed by Talip and coauthors (Talip et al., 2014). The annealing transient we consider is a heat up to roughly 1600 K in one hour, while the closest among the annealing transients performed by Talip and coauthors is a heat up to 1600 K in slightly less than one hour, followed by a holding of three hours at 1600 K. Talip and coauthors observed the peak of release rate at around 1500 K (compared to the 1200 K observed in our work, see Fig. 7b), and a total release at the end of the annealing of roughly 40% (compared with the 100% observed in our work, see Fig. 7a). This difference in the onset temperature of release can be connected to few differences between the experiments, e.g., the different grain size of the samples and the different technique used to introduce helium in the samples, i.e., infusion in our work and Pu-238 doping in the work of Talip and coauthors. This second aspect could mean that if the infusion process is not prolonged up to saturation, the helium concentration within the fuel grains could be non-uniform but concentrated towards the grain boundaries, i.e., being faster to release. This potential limitation of the infusion process calls for further investigations with modelling and experimental techniques able to describe the concentration field of helium within the grains themselves.

6. Conclusions and further developments

The methodology proposed in this work consists of three steps: (1) measurement of the grain-size distribution from SEM images of the UO_2 polycrystalline samples, (2) calculation of the helium distribution factor pertaining to each grain-size class after helium infusion, effectively distributing the initial helium concentration among grains of different size, and (3) simulation via SCIANTIX of the experimental annealing histories for each grain-size class, providing integral results averaged on the grain-size distribution.

Regarding the helium infusion process, the methodology proposed could be useful to predict the suitable experimental infusion time to reach saturation and calculate the helium solubility in polycrystalline samples, which is an important outcome of such experimental procedure and translates into a fundamental parameter of physics-based models describing helium behaviour. By considering the grain-size distribution, a better estimation of the proper infusion time to reach helium saturation in future helium infusion experiments can be achieved.

This treatment presents some limitations due to the uncertainties of the main modelling parameters, especially helium diffusivity and solubility, and due to missing model capabilities related to specific aspects of helium behaviour (i.e., helium bubble nucleation and the treatment of helium at grain boundaries), which are envisaged as future SCIANTIX developments. The effect of the fuel stoichiometry deviation on the helium diffusivity also has a significant impact and needs to be considered in future analyses.

Nevertheless, the proposed methodology to treat the grain-size distribution constitutes an added value compared to the current approach in physics-based models because the dynamics of helium release is more consistent with the physics of the fuel microstructure and can be applied for a more accurate design of future experiments. Furthermore, it can be suitable for application in fuel performance codes thanks to the overall limited computational requirement of the simulations (one simulation per grain-size class in which the grain-size distribution is discretized) and can be easily generalized to other gases (xenon and krypton), and other fuel microstructures as well. An example of worthwhile application of such methodology would be the modelling of fission gas behaviour in the high burnup structure (even if in this case the presence of high porosity implies the need of dedicated models), or in restructured fuel regions characterized by cylindrical grains. Moreover, the Cr-doped accident tolerant fuel concept seems an interesting application, given the peculiar grain-size distribution and its expected influence on inert gas behaviour (Cooper et al., 2021). Finally, it can also be adapted for fully ceramic fuel with a size distribution of spheres, for which the SCIANTIX code could also be applied to each class of spheres in combination with the concept of a surrounding buffer. This buffer can release fission products to the free volume upon saturation, depending on local burnup and temperature, or when certain transient conditions are fulfilled that may lead to cracking in the buffer layer.

Declaration of Competing Interest

The authors declare that they have no known competing financial interests or personal relationships that could have appeared to influence the work reported in this paper.

Data availability

Data will be made available on request.

Acknowledgements

This work has received funding from the Euratom research and training programme 2019-2020 under grant agreement No 945077 (PATRICIA Project) and from the Euratom research and training programme 2014–2018 through the INSPYRE Project under grant agreement No 754329.

Appendix. . Hypotheses on the modelling of the evolution of grain-size distribution.

The observation of the normalized quantile–quantile plots of the measured grain-size distributions in different stages along the experiment (Fig. A.1) indicates that limited change occurred in the shape of the grain-size during the grain growth process. Being aware that this result is far from general, we exploit it for this specific application assuming that the grain growth process for each grain size class of the distribution is proportional to the grain growth of the mean grain radius, thus:

$$D^i = \frac{\overline{D}}{\overline{D}_0} D_0^i \tag{A.1}$$

where D^i and D_0^i are the final and initial diameters in each grain size class, respectively, and $\overline{D}$ and $\overline{D}_0$ are the final and initial average diameters, respectively. Similar hypothesis is applied e.g., by El-Saied et al. (El-Saied and Olander, 1993).The results of the application of this hypothesis paired with the grain growth model proposed (Eq. (1) is reported in Fig. A.2.

References

Ainscough, J.B., Oldfield, B.W., Ware, J.O., 1973. Isothermal grain growth kinetics in sintered UO_2 pellets. J. Nucl. Mater. 49, 117–128. https://doi.org/10.1016/0022-3115(73)90001-9.

ASTM, 2018. Standard Test Methods for Determining Average Grain Size, pp. 1–27. https://doi.org/10.1520/E0112-12.1.4.

Barani, T., Pastore, G., Pizzocri, D., Andersson, D.A., Matthews, C., Alfonsi, A., Gamble, K.A., Van Uffelen, P., Luzzi, L., Hales, J.D., 2019. Multiscale modeling of fission gas behavior in U_3Si_2 under LWR conditions. J. Nucl. Mater. 522, 97–110. https://doi.org/10.1016/j.jnucmat.2019.04.037.

Botazzoli, P., Luzzi, L., Brémier, S., Schubert, A., Van Uffelen, P., Walker, C.T., Haeck, W., Goll, W., 2011. Extension and validation of the TRANSURANUS burn-up model for helium production in high burn-up LWR fuels. J. Nucl. Mater. 419, 329–338. https://doi.org/10.1016/j.jnucmat.2011.05.040.

P. Botazzoli, Helium Production and Behaviour in LWR Oxide Nuclear Fuels, PhD Thesis, Politec. Di Milano, Italy. (2011).

Bouëxière, D., Popa, K., Walter, O., Cologna, M., 2019. Kinetic study on the grain growth of PuO_2 nanocrystals. RSC Adv. 9, 6542–6547. https://doi.org/10.1039/c8ra10430a.

Cappia, F., Pizzocri, D., Schubert, A., Van Uffelen, P., Paperini, G., Pellottiero, D., Macian-Juan, R., Rondinella, V.V., 2016. Critical assessment of the pore size distribution in the rim region of high burnup UO\textsubscript{2} fuels. J. Nucl. Mater. 480, 138–149.

Cechet, A., Altieri, S., Barani, T., Cognini, L., Lorenzi, S., Magni, A., Pizzocri, D., Luzzi, L., 2021. A new burn-up module for application in fuel performance calculations targeting the helium production rate in (U, Pu)$_O$2 for fast reactors. Nucl. Eng. Technol. 53, 1893–1908. https://doi.org/10.1016/j.net.2020.12.001.

Cognini, L., 2021. Development of Experimental And Modelling Tools For Investigation Of Inert Gas Behaviour In Nuclear Materials. Politecnico di Milano. Master thesis.

Cognini, L., Pizzocri, D., Barani, T., Van Uffelen, P., Schubert, A., Wiss, T., Luzzi, L., 2018. Helium solubility in oxide nuclear fuel: Derivation of new correlations for Henry's constant. Nucl. Eng. Des. 340, 240–244. https://doi.org/10.1016/j.nucengdes.2018.09.024.

Cognini, L., Cechet, A., Barani, T., Pizzocri, D., Van Uffelen, P., Luzzi, L., 2021. Towards a physics-based description of intra-granular helium behaviour in oxide fuel for application in fuel performance codes. Nucl. Eng. Technol. 53 (2), 562–571.

L. Cognini, Investigation of helium behaviour in oxide nuclear fuel, PhD Thesis, Politecnico di Milano, Italy. (2021).

Colle, J.-Y., Maugeri, E.A., Thiriet, C., Talip, Z., Capone, F., Hiernaut, J.-P., Konings, R.J.M., Wiss, T., 2014. A mass spectrometry method for quantitative and kinetic analysis of gas release from nuclear materials and its application to helium desorption from UO_2 and fission gas release from irradiated fuel. J. Nucl. Sci. Technol. 51 (5), 700–711.

Cooper, M.W., Pastore, G., Che, Y., Matthews, C., Forslund, A., Stanek, C.R., Shirvan, K., Tverberg, T., Gamble, K.A., Mays, B., Andersson, D.A., 2021. Fission gas diffusion and release for Cr_2O_3-doped UO_2: From the atomic to the engineering scale. J. Nucl. Mater. 545, 152590 https://doi.org/10.1016/j.jnucmat.2020.152590.

Crank, J., Gupta, R.S., 1975. Isotherm migration method in two dimensions. Int. J. Heat Mass Transf. 18, 1101–1107. https://doi.org/10.1016/0017-9310(75)90228-8.

De Bona, E., Balice, L., Cognini, L., Holzhäuser, M., Popa, K., Walter, O., Cologna, M., Prieur, D., Wiss, T., Baldinozzi, G., 2021. Single-step, high pressure, and two-step spark plasma sintering of UO_2 nanopowders. J. Eur. Ceram. Soc. 41 (6), 3655–3663.

El-Atwani, O., Nathaniel, J.E., Leff, A.C., Muntifering, B.R., Baldwin, J.K., Hattar, K., Taheri, M.L., 2017. The role of grain size in He bubble formation: Implications for swelling resistance. J. Nucl. Mater. 484, 236–244. https://doi.org/10.1016/j.jnucmat.2016.12.003.

El-Saied, U.M., Olander, D.R., 1993. Fission gas release during grain growth in a microstructure with a distribution of grain sizes. J. Nucl. Mater. 207, 313–326.

C. Ferry, J. Piron, A. Ambard, Effect of helium on the microstructure of spent fuel in a repository: An operational approach, 407 (2010) 100–109. 10.1016/j.jnucmat.2010.09.034.

GIF (Generation IV International Forum), Annual Report, NEA No. 7527, OECD 2020, 2019. www.gen-4.org/gif/jcms/c_119024/gif-2019-annual-report.

European Commission, 2022. Joint Research Centre, Directorate G - nuclear safety & security, Karlsruhe, Germany. TRANSURANUS Handbook.

Giorgi, R., Cechet, A., Cognini, L., Magni, A., Pizzocri, D., Zullo, G., Schubert, A., Van Uffelen, P., Luzzi, L., 2022. Physics-based modelling and validation of inter-granular helium behaviour in SCIANTIX. Nucl. Eng. Technol. 54, 2367–2375. https://doi.org/10.1016/j.net.2022.01.012.

Govers, K., Lemehov, S., Hou, M., Verwerft, M., 2009. Molecular dynamics simulation of helium and oxygen diffusion in $UO_{2\pm x}$. J. Nucl. Mater. 395, 131–139. https://doi.org/10.1016/j.jnucmat.2009.10.043.

Ham, F.S., 1958. Theory of diffusion-limited precipitation. J. Phys. Chem. Solids. 6 (4), 335–351.

Jomard, G., Struzik, C., Boulore, A., Mailhé, P., Auret, V., Largenton, R., 2014. CARACAS: an Industrial Model for the Description of Fission Gas Behavior in LWR-UO2 Fuel. In: 2014 Proc. Water React Fuel Perform. Meet., pp. 14–17.

Lösönen, P., 2000. On the behaviour of intragranular fission gas in UO_2 fuel. J. Nucl. Mater. 280, 56–72. https://doi.org/10.1016/S0022-3115(00)00028-3.

Luzzi, L., Cognini, L., Pizzocri, D., Barani, T., Pastore, G., Schubert, A., Wiss, T., Van Uffelen, P., 2018. Helium diffusivity in oxide nuclear fuel: Critical data analysis and new correlations. Nucl. Eng. Des. 330 https://doi.org/10.1016/j.nucengdes.2018.01.044.

Maugeri, E., Wiss, T., Hiernaut, J.P., Desai, K., Thiriet, C., Rondinella, V.V., Colle, J.Y., Konings, R.J.M., 2009. Helium solubility and behaviour in uranium dioxide. J. Nucl. Mater. 385, 461–466. https://doi.org/10.1016/j.jnucmat.2008.12.033.

Mendelson, M.I., 1969. Average grain size in polycrystalline ceramics. J. Am. Ceram. Soc. 52, 443–446. https://doi.org/10.1111/j.1151-2916.1969.tb11975.x.

Miao, Y., Yao, T., Lian, J., Park, J.S., Almer, J., Bhattacharya, S., Yacout, A.M., Mo, K., 2017. In situ synchrotron investigation of grain growth behavior of nano-grained UO_2. Scr. Mater. 131, 29–32. https://doi.org/10.1016/j.scriptamat.2016.12.025.

Millett, P.C., Zhang, Y., Tonks, M.R., Biner, S.B., 2013. Consideration of grain size distribution in the diffusion of fission gas to grain boundaries. J. Nucl. Mater. 440, 435–439. https://doi.org/10.1016/j.jnucmat.2013.05.065.

Noirot, L., 2006. MARGARET: An advanced mechanistic model of fission gas behavior in nuclear fuel. J. Nucl. Sci. Technol. 43, 1149–1160. https://doi.org/10.1080/18811248.2006.9711207.

Olander, D.R., 1976. Division of Reactor Development and Demonstration., U.S. Atomic Energy Commission, Fundamental aspects of nuclear reactor fuel elements: prepared for the Division of Reactor Development and Demonstration. Energy Research and Development Administration.

Parks, C., Koswara, A., Devilbiss, F., Tung, H.H., Nere, N.K., Bordawekar, S., Nagy, Z.K., Ramkrishna, D., 2017. Solubility curves and nucleation rates from molecular dynamics for polymorph prediction-moving beyond lattice energy minimization. Phys. Chem. Chem. Phys. 19, 5285–5295. https://doi.org/10.1039/c6cp07181c.

Parrish, R., Aitkaliyeva, A., 2018. A review of microstructural features in fast reactor mixed oxide fuels. J. Nucl. Mater. https://doi.org/10.1016/j.jnucmat.2018.05.076.

Pastore, G., Luzzi, L., Di Marcello, V., Van Uffelen, P., 2013. Physics-based modelling of fission gas swelling and release in UO_2 applied to integral fuel rod analysis. Nucl. Eng. Des. 256, 75–86. https://doi.org/10.1016/j.nucengdes.2012.12.002.

Pastore, G., Swiler, L.P., Hales, J.D., Novascone, S.R., Perez, D.M., Spencer, B.W., Luzzi, L., Van Uffelen, P., Williamson, R.L., 2015. Uncertainty and sensitivity analysis of fission gas behavior in engineering-scale fuel modeling. J. Nucl. Mater. 456, 398–408. https://doi.org/10.1016/j.jnucmat.2014.09.077.

Pizzocri, D., Barani, T., Luzzi, L., 2020. SCIANTIX: A new open-source multi-scale code for fission gas behaviour modelling designed for nuclear fuel performance codes. J. Nucl. Mater. 532, 152042.

D. Pizzocri, T. Barani, L. Luzzi, Coupling of TRANSURANUS with the SCIANTIX fission gas behaviour module, in: Int. Work. " Towar. Nucl. Fuel Model. Var. React. Types across Eur., 2019.

Rufeh, F., Olander, D.R., Pigford, T.H., 1965. The Solubility of Helium in Uranium Dioxide. Nucl. Sci. Eng. 23, 335–338. https://doi.org/10.13182/nse65-a21069.

Sauvage, T., Desgardin, P., Martin, G., Garcia, P., Carlot, G., Labrim, H., Khodja, H., Moretto, P., Barthe, M.F., Blondiaux, G., Erramli, H., Piron, J.P., 2005. Microstructure effects on He diffusion in sintered UO_2 by μnRA. Nucl. Instrum. Methods Phys. Res. Sect. B Beam Interact. Mater. Atoms. 240, 271–276. https://doi.org/10.1016/j.nimb.2005.06.128.

Schwartz, A.J., Wall, M.A., Zocco, T.G., Wolfer, W.G., 2005. Characterization and modelling of helium bubbles in self-irradiated plutonium alloys. Philos. Mag. 85, 479–488. https://doi.org/10.1080/02678370412331320026.

Spino, J., Vennix, K., Coquerelle, M., 1996. Detailed characterisation of the rim microstructure in PWR fuels in the burn-up range 40–67 GWd/t_{HM}. J. Nucl. Mater. 231, 179–190. https://doi.org/10.1016/0022-3115(96)00374-1.

Sung, P., 1967. Equilibrium Solubility And Diffusivity Of Helium In Single-Crystal Uranium Dioxide. Univ. Washingt. PhD Thesis,.

Sung, P., Turnbaugh, J.E., 1968. Calculation of diffusivity and solubility with error analysis for diffusion in a sphere. J. Appl. Phys. 39, 346–347. https://doi.org/10.1063/1.1655761.

Talip, Z., Wiss, T., Maugeri, E.A., Colle, J.Y., Raison, P.E., Gilabert, E., Ernstberger, M., Staicu, D., Konings, R.J.M., 2014. Helium behaviour in stoichiometric and hyper-stoichiometric UO_2. J. Eur. Ceram. Soc. 34, 1265–1277. https://doi.org/10.1016/j.jeurceramsoc.2013.11.032.

Talip, Z., Wiss, T., Di Marcello, V., Janssen, A., Colle, J.Y., Van Uffelen, P., Raison, P., Konings, R.J.M., 2014. Thermal diffusion of helium in ^{238}Pu-doped UO_2. J. Nucl. Mater. 445, 117–127. https://doi.org/10.1016/j.jnucmat.2013.10.066.

Tonks, M.R., Andersson, D., Phillpot, S.R., Zhang, Y., Williamson, R., Stanek, C.R., Uberuaga, B.P., Hayes, S.L., 2017. Mechanistic materials modeling for nuclear fuel performance. Ann. Nucl. Energy. 105, 11–24. https://doi.org/10.1016/J.ANUCENE.2017.03.005.

Tonks, M.R., Simon, P.C.A., Hirschhorn, J., 2021. Mechanistic grain growth model for fresh and irradiated UO2 nuclear fuel. J. Nucl. Mater. 543, 152576 https://doi.org/10.1016/j.jnucmat.2020.152576.

Van Brutel, L., Chartier, A., 2019. A new equation of state for helium nanobubbles embedded in UO_2 matrix calculated via molecular dynamics simulations. J. Nucl. Mater. 518, 431–439. https://doi.org/10.1016/j.jnucmat.2019.02.015.

Van Uffelen, P., Pastore, G., Di Marcello, V., Luzzi, L., 2011. Multiscale modelling for the fission gas behaviour in the TRANSURANUS Code. Nucl. Eng. Technol. 43 (6), 477–488.

Van Uffelen, P., Botazzoli, P., Luzzi, L., Bremier, S., Schubert, A., Raison, P., Eloirdi, R., Barker, M.A., 2013. An experimental study of grain growth in mixed oxide samples with various microstructures and plutonium concentrations. J. Nucl. Mater. 434, 287–290. https://doi.org/10.1016/j.jnucmat.2012.11.053.

Verdolin, F., Novascone, S., Pizzocri, D., Pastore, G., Barani, T., Luzzi, L., 2021. Modelling fission gas behaviour in fast reactor (U, Pu)$_O$2 fuel with BISON. J. Nucl. Mater. 547 https://doi.org/10.1016/j.jnucmat.2020.152728.

Veshchunov, M.S., 2000. On the theory of fission gas bubble evolution in irradiated UO_2 fuel. J. Nucl. Mater. 277, 67–81. https://doi.org/10.1016/S0022-3115(99)00136-1.

Veshchunov, M.S., Dubourg, R., Ozrin, V.D., Shestak, V.E., Tarasov, V.I., 2007. Mechanistic modelling of urania fuel evolution and fission product migration during

irradiation and heating. J. Nucl. Mater. 236, 179–200. https://doi.org/10.1016/j.jnucmat.2007.01.081.

Williamson, R.L., Gamble, K.A., Perez, D.M., Novascone, S.R., Pastore, G., Gardner, R.J., Hales, J.D., Liu, W., Mai, A., 2016. Validating the BISON fuel performance code to integral LWR experiments. Nucl. Eng. Des. 301, 232–244. https://doi.org/10.1016/j.nucengdes.2016.02.020.

Yakub, E., Ronchi, C., Staicu, D., 2010. Diffusion of helium in non-stoichiometric uranium dioxide. J. Nucl. Mater. 400, 189–195. https://doi.org/10.1016/j.jnucmat.2010.03.002.

Yao, T., Mo, K., Yun, D., Nanda, S., Yacout, A.M., Lian, J., 2017. Grain growth and pore coarsening in dense nano-crystalline UO_{2+x} fuel pellets. J. Am. Ceram. Soc. 100, 2651–2658. https://doi.org/10.1111/jace.14780.